

Article

Influence of a Novel Double Tempering Process on the Microstructure and Mechanical Properties of Cu-Alloyed Austempered Ductile Iron with Possible Nano (Micro)-Characterization Using Neutron Beam Techniques

Nikša Čatipović ^{1,*} , Massimo Rogante ² , Hasan Avdušinić ³ and Karla Grgić ¹

¹ Faculty of Electrical Engineering, Mechanical Engineering and Naval Architecture, University of Split, 21000 Split, Croatia

² Rogante Engineering Office, Contrada San Michele n. 61, 62012 Civitanova Marche, Italy

³ Faculty of Metallurgy and Technology, University of Zenica, 72000 Zenica, Bosnia and Herzegovina

* Correspondence: ncatipov@fesb.hr

Abstract: In this paper, a novel method for the double heat treatment of ductile iron was applied. Ten sets of specimens (three specimens in each set) of ductile cast iron (DCI) containing 0.51% wt. Cu were prepared and converted to austenitic ductile iron. All specimens were austenitized at 850 °C for 60 min and annealed at 420 °C, 331 °C and 250 °C for 120, 68 and 30 min, respectively. Five sets of samples were then annealed at 500 °C for 60 min, creating a novel double heat treatment process for annealing. Finally, all specimens were slowly cooled in air at ambient temperature. Tensile strength, hardness and elongation were measured in all specimens to compare the specimens with and without subsequent tempering. A microstructural analysis was also performed, which showed that the microstructure changed for the specimens that were subsequently tempered with. The results show that specimens with subsequent tempering have slightly higher hardness, a small decrease in tensile strength and significantly higher elongation. In addition, specimens with subsequent tempering exhibit more uniform mechanical properties compared to specimens without subsequent tempering. The use of neutron beam techniques was proposed to further characterize the newly formed microstructure after subsequent tempering.

Keywords: austempered ductile iron; novel double tempering; mechanical properties; nano(micro)-characterization; neutron beam techniques



Citation: Čatipović, N.; Rogante, M.; Avdušinić, H.; Grgić, K. Influence of a Novel Double Tempering Process on the Microstructure and Mechanical Properties of Cu-Alloyed Austempered Ductile Iron with Possible Nano (Micro)-Characterization Using Neutron Beam Techniques. *Crystals* **2023**, *13*, 1359. <https://doi.org/10.3390/cryst13091359>

Academic Editors: Subbarayan Sivasankaran and Vladimir I. Zverev

Received: 9 August 2023

Revised: 25 August 2023

Accepted: 6 September 2023

Published: 8 September 2023



Copyright: © 2023 by the authors. Licensee MDPI, Basel, Switzerland. This article is an open access article distributed under the terms and conditions of the Creative Commons Attribution (CC BY) license (<https://creativecommons.org/licenses/by/4.0/>).

1. Introduction

DCI—nodular or spherulitic—is a special form of cast iron which incorporates the positive properties of both cast steel (higher strength and toughness) and grey cast iron (favourable castability) [1]. DCI is among the economically viable materials subject to increasing demand. It has inherently more favourable mechanical properties compared to grey cast iron, and with heat treatment (HT) it can achieve much better properties [2–9]. Austempering DCI generates austempered ductile iron (ADI). This cast iron has a special microstructure called ausferrite, composed of carbon-enriched retained austenite and needle ferrite [10–12]. A major advantage of ADI is that it has double the strength of conventional HT with the same ductility. Depending on the alloying elements of DCI and the HT parameters (austempering temperature and time), a range of mechanical properties can be obtained. ADI expresses better properties than many aluminium and iron alloys [13].

DCI austempering is like steel austempering, only different microstructure and properties are obtained [14–16]. The large amount of silicon in DCI affects the microstructural differences, which limits the formation of carbides [17–19].

The austenitizing temperature ranges from 850 to 950 °C [20]. Chemical composition and casting size affect the austenitizing time. After reaching the austenitizing temperature,

DCI is immersed in a hot salt bath for a certain time until the transformation is completed. The temperature of the salt bath ranges from 230 to 450 °C. An increase in the bath temperature decreases the final strength and hardness of ADI. The salt bath temperature and DCI chemical composition determine the specimens' quenching time [21].

After austempering, i.e., annealing at 500 °C for 60 min, an HT was set up. Such an HT generally removes residual stresses (RS) and elevates toughness. Subsequent tempering duration and temperature attempt to optimize final specimen properties.

To avoid RS, ADI must be immediately tempered after bath quenching. High-temperature DCI tempering is performed in two steps. In the first step, carbide precipitation occurs as in steel. In the second step, retained austenite decomposes and from carbides small, secondary graphite occurs, resulting in pearlite formation. Secondary graphitization leads to a decrease in tensile strength. Considering that the alloying elements' weight fraction influences secondary graphitization, each alloying element has its own tempering range.

In this work, double heat-treated specimens (five sets of DCI specimens containing 0.51 wt% Cu) were tested to determine their tensile strength and elongation. Hardness was also measured and their microstructure was analysed. The average results obtained were compared to five sets of specimens (with the same weight percentage of Cu) that were only annealed (with the same parameters) without being subsequently tempered.

Microstructural analysis was performed and the volume fraction of the retained austenite was measured in all samples. Since a new microstructure developed as a result of the novel double annealing, a detailed microstructural characterization using a neutron beam technique was proposed. It was found that neutron beam characterization gave good results in determining RS in ADI [22–25].

2. Materials and Methods

In this work, 5 sets of specimens of DCI were fabricated, austempered and then high-temperature tempered. In addition, 5 sets of specimens were prepared and HT without high-temperature tempering to allow for comparison with the previous specimens. The exact chemical composition of the DCI is as follows: 3.63 wt% C, 2.61 wt% Si, 0.135 wt% Mn, 0.51 wt% Cu, 0.0035 wt% S, 0.022 wt% P, 0.005 wt% Cr, 0.004 wt% V, 0.085 wt% Ni, 0.003 wt% Mo, 0.017 wt% Al, 0.013 wt% Ti, 0.033 wt% Sn, 0.017 wt% W, and 0.041 wt% Mg. The DCI specimens were prepared according to the ISO 6892-1:2009 standard, Figure 1a. Figure 1b shows the initial microstructure of the DCI used in this work.

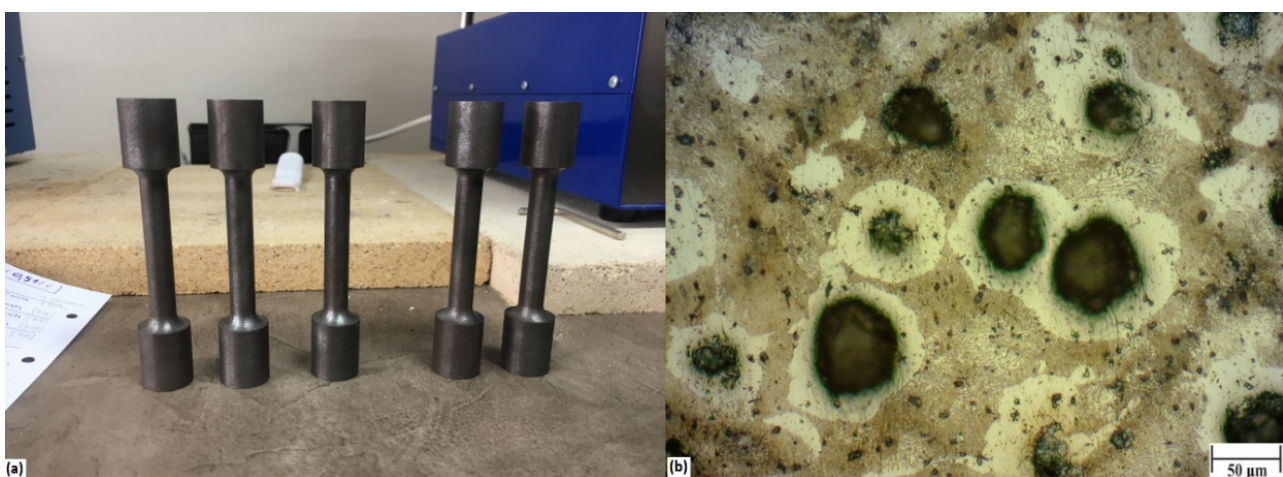


Figure 1. (a) One DCI specimen from each set before heat treatment; (b) Initial microstructure of the ductile iron specimens under 200× magnification.

The DCI specimens were first austenitized at 850 °C for 60 min and then annealed (three specimens with different annealing temperatures and times). After austenitizing,

5 sets of specimens were tempered at 500 °C for 60 min. Table 1 shows the HT parameters for each set of specimens.

Table 1. Heat treatment parameters for each set of specimens.

Specimen Set ID		Austempering Parameters	
Without Subsequent Tempering	With Subsequent Tempering	Temperature, T_a [°C]	Time, t_a [min]
705	719	250	30
715	720	250	120
706	721	331	68
718	722	420	30
709	724	420	120

The specimen austenitization was completed using an Estherm DEMITERM Easy9 laboratory furnace with a type K thermocouple. Immediately after austenitizing, the specimens were quenched in a salt bath to form ADI. Austempering was conducted from 250 to 420 °C, with austempering times ranging from 30 to 120 min [26]. Cooling of all specimens to ambient temperature was performed in air. A JPA 6-600 furnace with type K thermocouple was used for austempering. AS 140 salt was used (50% NaNO₃ and 50% KNO₃) [27]. Figure 2 shows the salt bath furnace in which the samples were annealed (a) and the thermocouple immersed in the salt bath for more accurate control of the salt bath temperature (b).

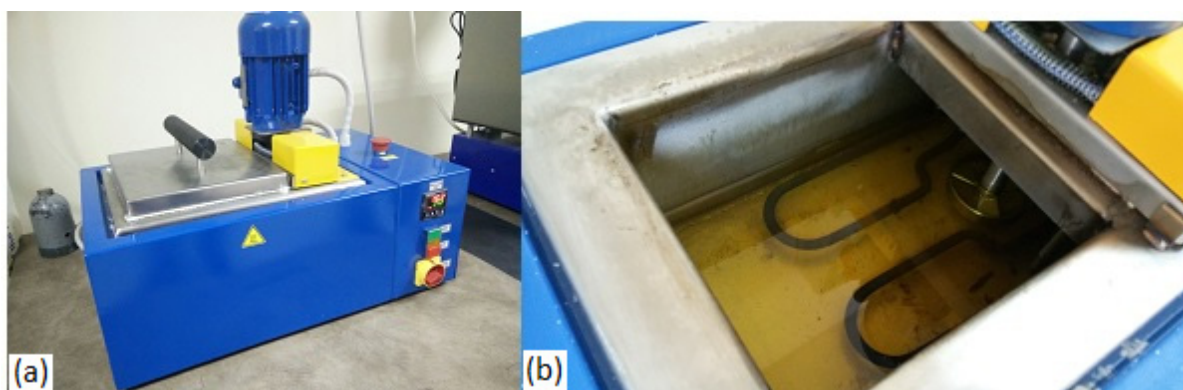


Figure 2. (a) Austempering salt bath; (b) thermal element submerged in the salt bath.

Subsequent tempering was performed after the previous HT using a ZLATARNA-CELJE laboratory furnace. Figure 3 shows the appearance of one specimen from each set after subsequent tempering.

In order to analyse the microstructure of the specimens, they had to be thoroughly ground and polished and then chemically etched. The specimens were first ground on a “Handimet Grinder” on a 600 fineness water track. Then, they were polished on a polishing wheel, using aluminium oxide particles (Al₂O₃) in aqueous suspension as the abrasive. The final surface preparation was done by etching the surface with Nital, which is obtained by mixing 5% nitric acid with 70% ethanol alcohol. The etching time for each sample was 5 s. The specimens were viewed using a vertical light microscope “OPTON Axioskop” with interchangeable lenses. The “DinoEye Eyepiece” digital camera microscope was connected via USB to a computer equipped with “DINOCAPTURE 2.0” software for viewing and analysing the images.

To determine the volume fraction of retained austenite in the samples, the metallographic images were analysed using the open source ImageJ software. First, IrfanView software was used to sharpen images, then they were uploaded to ImageJ and converted to black and white. Then, all black areas representing graphite nodules were eliminated

and white ferrite was removed from the rest of the image to obtain a volume fraction of residual austenite. For each elimination of graphite and ferrite, the same values were used for the selection of the black and white spectra to ensure reproducibility in the analysis of all microstructural images.



Figure 3. One ADI specimen from each set after high-temperature tempering.

Hardness was tested on a stationary universal hardness testing machine “Dia Testor 2 RC-S Wolpert” using the Vickers method with an indentation force of $F = 98.1 \text{ N}$ (10 kp).

The tensile strength of specimens was examined using a “WOLPERT 20 TUZ 750” universal tensile testing machine with a 200 kN maximum force.

3. Results

3.1. Microstructure

Figures 4–13 show that $200\times$ and $500\times$ magnifications were used and metallographic images were taken. The metallographic examination of the specimens followed by tempering again showed that the material is isotropic and the metallography of all specimens is uniform. Spheroidal graphite and the ausferrite phase of the ADI alloy can be seen in the metallographic images [28]. The isotropic nature of the material and its uniformity over the entire cross-section are visible. The microstructures of all specimens in a set are similar, which is also confirmed through the measured mechanical properties.

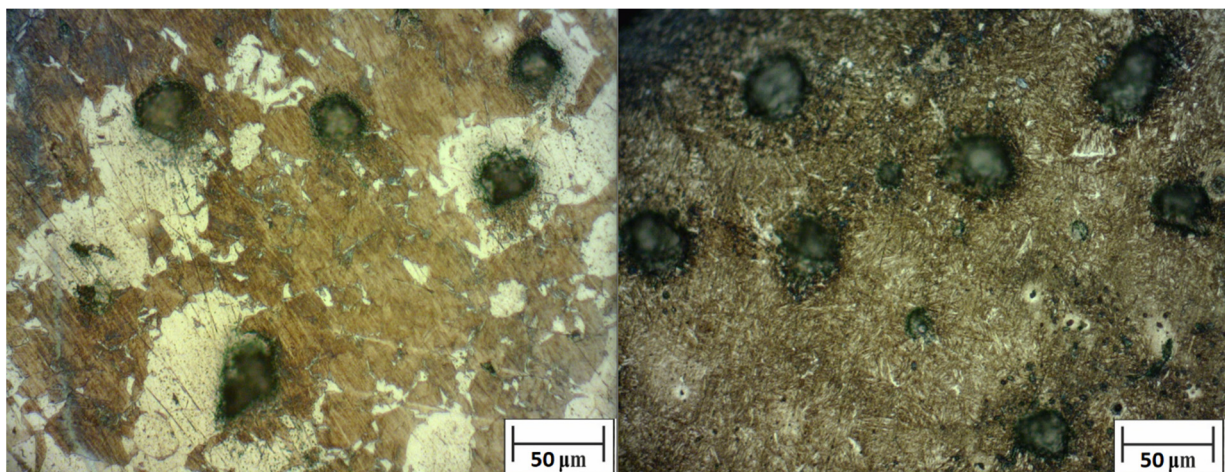


Figure 4. Microstructure comparison of specimen sets 705 and 719 under $200\times$ magnification.

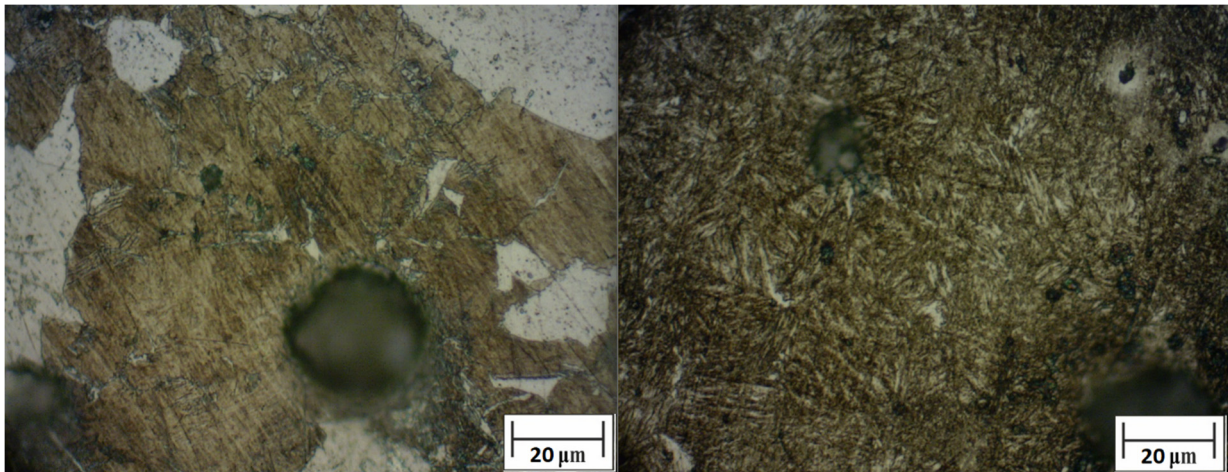


Figure 5. Microstructure comparison of specimen sets 705 and 719 under 500× magnification.

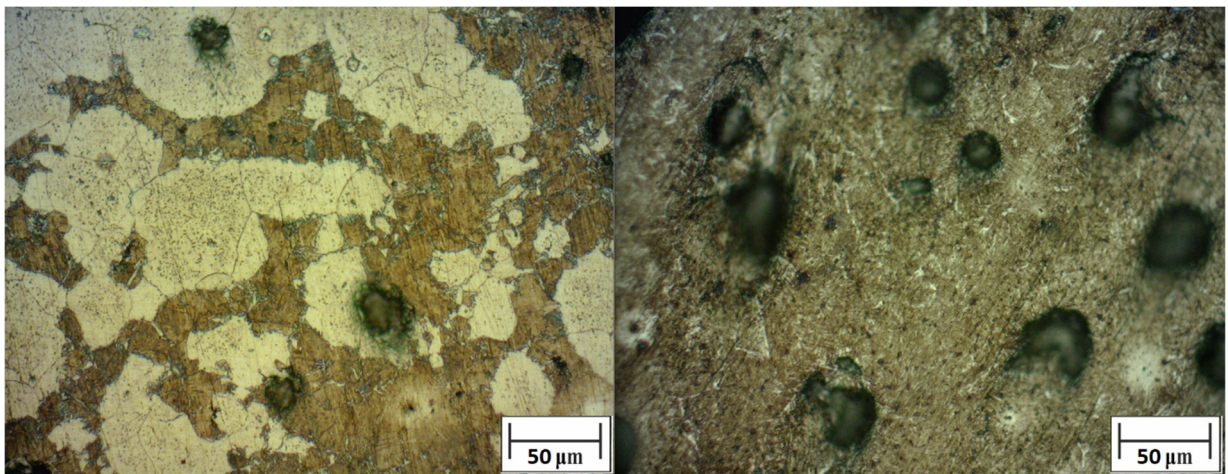


Figure 6. Microstructure comparison of specimen sets 715 and 720 under 200× magnification.

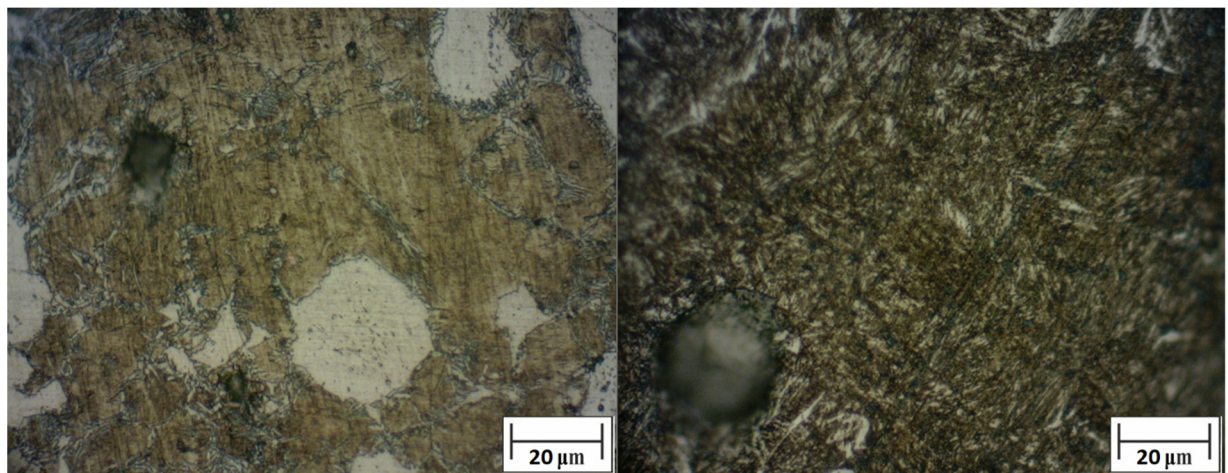


Figure 7. Microstructure comparison of specimen sets 715 and 720 under 500× magnification.

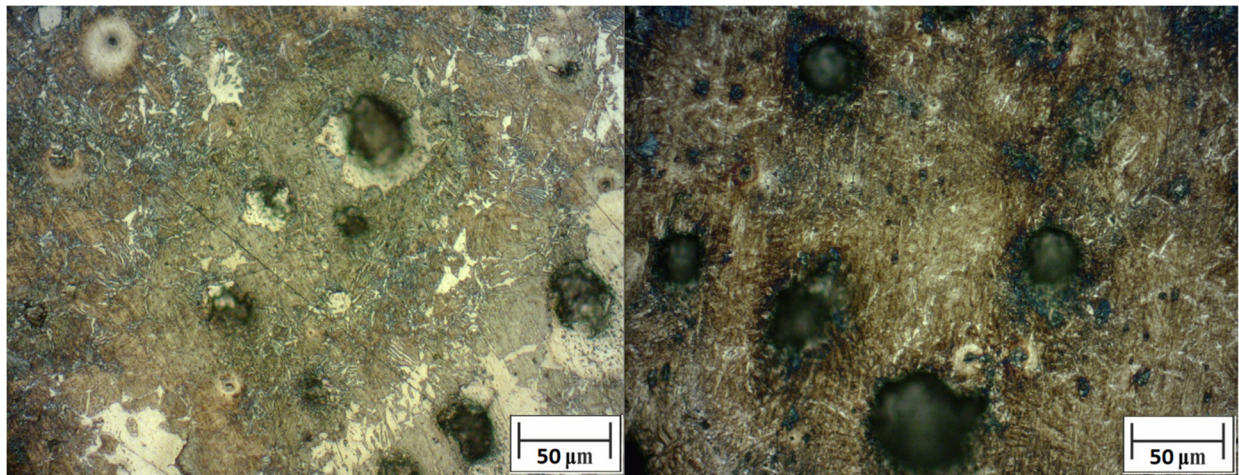


Figure 8. Microstructure comparison of specimen sets 706 and 721 under 200× magnification.

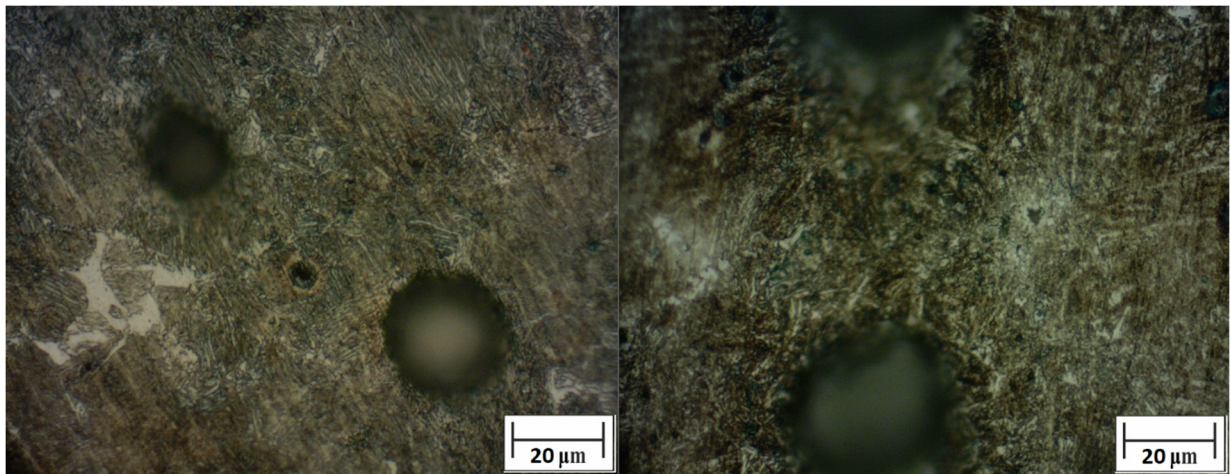


Figure 9. Microstructure comparison of specimen sets 706 and 721 under 500× magnification.

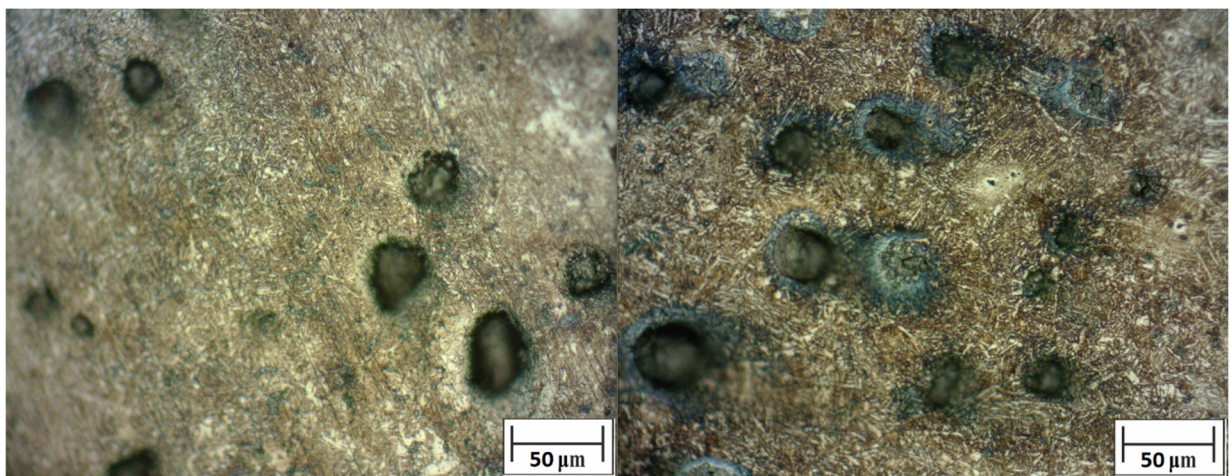


Figure 10. Microstructure comparison of specimen sets 718 and 722 under 200× magnification.

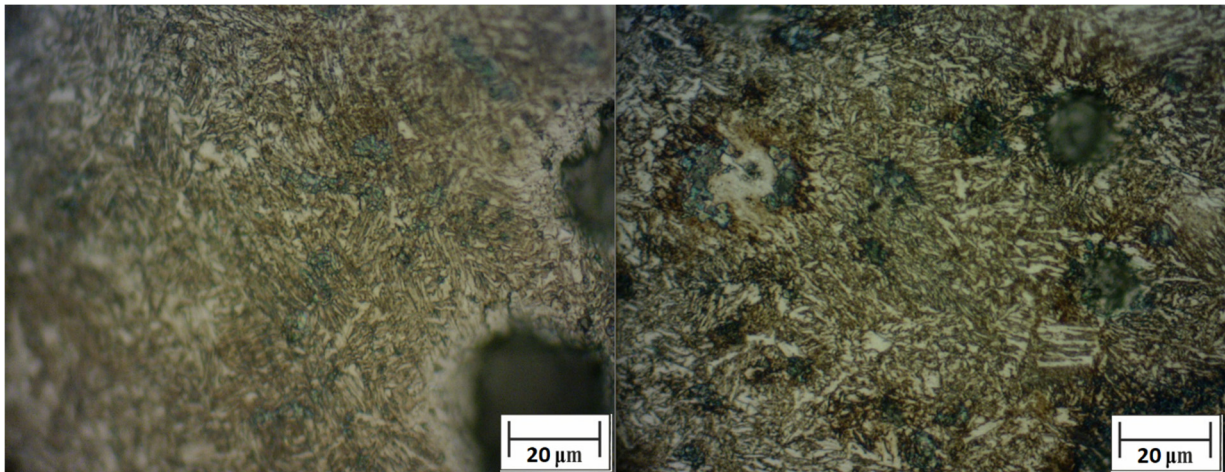


Figure 11. Microstructure comparison of specimen sets 718 and 722 under 500× magnification.

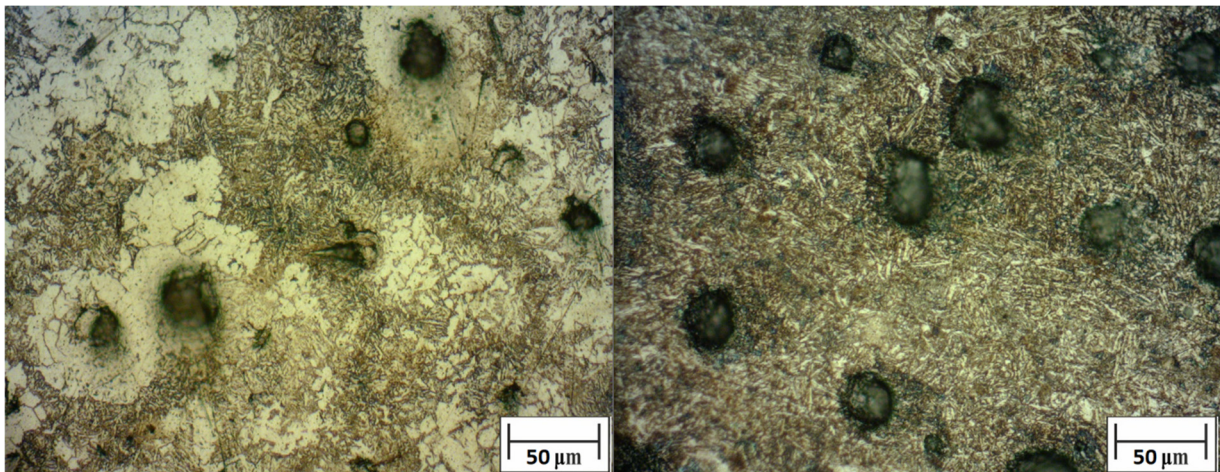


Figure 12. Microstructure comparison of specimen sets 709 and 724 under 200× magnification.

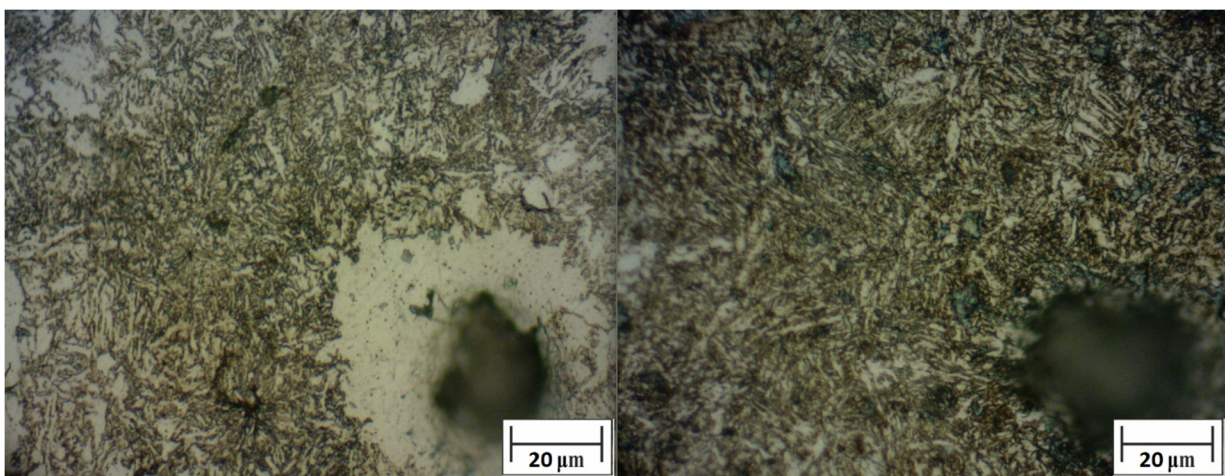


Figure 13. Microstructure comparison of specimen sets 709 and 724 under 500× magnification.

Phases of ausferrite and graphite spheres are visible under all magnifications. Indeed, the microstructure of the specimens with subsequent tempering is more acicular, while the specimens without subsequent tempering have a more plate-like character [29]. In addition, ferrite phases are also visible in the material at $500\times$ magnification for specimens without subsequent tempering, in contrast to specimens with subsequent tempering where ferrite phases are minimal. This ferrite is referred to as allotriomorphic, or elongated ferrite. Subsequent annealing resulted in a more uniform (homogeneous) structure between different samples, which is confirmed by the results yielding better (optimal) mechanical properties [30]. It is assumed that the elongated ferrite started to decompose during subsequent annealing and partially transformed into pearlite and carbides due to carbon diffusion, which is why there was an improvement in hardness and elongation and a slight decrease in tensile strength for the specimen sets 719, 720 and 721, while tensile strength increased for specimen sets 722 and 724.

The aim of the metallographic analysis was to determine the volume fraction of retained austenite in the microstructure of all samples. The volume fraction of retained austenite after HT significantly affects the mechanical properties of the material [30,31].

For each specimen in a set, three microstructural images were taken at the same magnification and analysed. The mean values of the retained austenite for each set of specimens were calculated and are shown in Table 2.

Table 2. Mean values of volume fraction of retained austenite results for each set.

Without Subsequent Tempering		With Subsequent Tempering	
Specimen Set ID	Vol. [%]	Specimen Set ID	Vol. [%]
705	30	719	19
715	34	720	21
706	51	721	22
718	56	722	16
709	24	724	14

Cu is used as an influencing element for the formation of pearlite in castings with high strength and good workability [32]. It is added when it is necessary to achieve the fully pearlitic microstructure of a DCI. Although the solubility of Cu in Fe is about 2.5%, the Cu content in pearlite DCI should be between 0.4% and 0.8%. In addition to reducing toughness, Cu increases the transition temperature, increases tensile strength and hardness and has a positive effect on hardenability. Cu as an alloying element prevents the formation of carbides in an ADI, but has no effect on the diffusion of C into the austenite or its stability. Cu increases the transformation rate and the C content of the matrix during austenitization and enlarges the austenitic zone in the phase diagram of the transformation. The addition of Cu delays the reaction of the second transformation stage, which prevents the deterioration of mechanical properties. This is a consequence of the richer initial microstructure of DCI with pearlite and carbides, whose decomposition enriches the residual austenite during HT and promotes its formation [33,34].

3.2. Hardness

Five measurements were taken from each sample within each set, from which the mean values were calculated, Table 3.

The results obtained show that the hardness increased for all samples with a subsequent increase in temperature. The greatest change in hardness is observed in specimen set 721 compared to specimen set 706: 86 HV. Sample set 719 has the highest hardness and specimen set 722 has the lowest hardness. The reason for the increase in hardness is the formation of secondary carbides in the microstructure due to C diffusion from decomposed ausferrite during the secondary tempering process. These carbides are relatively small and uniformly distributed in the microstructure, as can be seen from the micrographs, which increases hardness.

Table 3. Vickers hardness mean values for each set.

Without Subsequent Tempering		With Subsequent Tempering	
Specimen Set ID	Hardness [HV 10]	Specimen Set ID	Hardness [HV 10]
705	318	719	342
715	300	720	326
706	242	721	328
718	212	722	296
709	238	724	298

3.3. Tensile Strength and Elongation

A comparison of the average results for tensile strength and elongation with and without subsequent tempering is shown in Table 4.

Table 4. Mean tensile strength and elongation results for each set.

Without Subsequent Tempering			With Subsequent Tempering		
Specimen Set ID	Tensile Strength, R_m [MPa]	Elongation, ϵ_k [%]	Specimen Set ID	Tensile Strength, R_m [MPa]	Elongation, ϵ_k [%]
705	1240	1.3	719	1023	14.5
715	1184	2.1	720	901	19.2
706	927	5.0	721	814	21.0
718	693	10.1	722	940	30.2
709	852	1.1	724	980	25.1

Specimen set 719 was measured to have a maximum tensile strength of 1023 MPa and the lowest elongation, obtained at 250 °C and 30 min. Specimen set 721 has the lowest tensile strength of 814 MPa, austempered at 331 °C for 68 min. The highest elongation of 30.2% was measured in specimen set 722, which was annealed at 420 °C for 30 min.

For specimen set 719, compared to specimen set 705, tensile strength decreases by 217 MPa, while elongation increases. A decrease in tensile strength is also observed for specimen sets 720 and 721 compared to specimen sets 715 and 706. Similarly, as before, elongation increases. For specimen sets 718 and 709, austempered at 420 °C, tensile strength decreases compared to specimen sets 722 and 724. Specimen set 718 was austempered 30 min and obtained 10.1% elongation. Austempering specimen set 709 for 120 min resulted in 1.1% elongation. It is clear that a longer austempering time at a higher temperature decreases the elongation of the material, which can be explained by the second stage of transformation and the decomposition of ausferrite. In the case of specimen sets 722 and 724, the subsequent tempering had a positive effect; both elongation and tensile strength have increased.

From all the results is clear that increasing austempering temperature will decrease tensile strength, but after subsequent high tempering, the tensile strength can increase again. An increase in austempering temperature will also increase elongation but as seen in specimen set 724, with an austempering time of 120 min, elongation will decrease, although the result was still good compared to specimen set 709, which was not tempered.

4. Characterization

ADI is suitable for numerous applications where it is essential to detect the presence of defects in the material (even below the surface) and to determine the exact metallographic structure. Neutron beam techniques (NBT), which are non-destructive and non-invasive, are particularly useful for interpreting the structural basis for physical properties and improving the quality of the material under consideration. They make it possible to determine directly on real samples the parameters that are partly responsible for the macroscopic prop-

erties and the final performances. Special measurement and data processing techniques have been developed for these assessments by the Rogante Engineering Office [35,36].

In particular, small-angle neutron scattering (SANS), which is suitable for micro- and nano-level characterization [37], allows for obtaining information about the inhomogeneities present (defects such as pores, precipitates and gas bubbles) and identifying the phase separations. This technique has the same theoretical basis as small-angle X-ray scattering, but it is limited due to the low penetrating power of X-rays. It consists of expanding a neutron beam after passing it through the sample containing the heterogeneities. The scattering angles considered must be larger than λ/R , where R is the largest dimension of the inhomogeneities and λ is the wavelength of the neutron beam. Specific approximation models of the obtained analytical data allow for deriving the distribution function of the size of the inhomogeneities, together with data on the amount, volume fraction and shape of the considered defects. The distribution of shapes can generally be evaluated in the range of $100 \div 104 \text{ \AA}$. This SANS method, which provides information with a high degree of statistical precision since it is based on a macroscopic sample volume between mm^3 and cm^3 , is certainly complementary to both optical and electronic microscopy (the latter can analyse only part of the area with very small dimensions). SANS would be useful to further characterise the newly formed microstructure after subsequent annealing.

The retained austenite contained in the austenite that makes up the ADI cast iron may be more or less saturated with carbon, which affects the quality of the material. Diffraction techniques, e.g., X-ray diffraction, have already been used in these cases to study the morphology of cavitation-damaged surfaces and microstructural changes in ADI cast iron samples at $300 \text{ }^\circ\text{C}$ and $400 \text{ }^\circ\text{C}$ and with ausferrite microstructures with 16% and 31.4% residual austenite [38]. High-resolution powder diffraction followed by a standard Rietveld refinement (in addition to phase quantification using pole figure measurements and Bragg edge neutron transmission) have been used to determine the strain-induced martensite content [24].

In our case, neutron diffraction (ND) [39] can also help to determine the retained austenite content—e.g., by comparison as a function of an applied stress and strain state—with satisfactory accuracy, even for mass fractions of austenite below 0.01%.

Finally, a good prediction of the evolution of the nano-(micro-)structure after the HTs can be achieved by developing appropriate models based on investigations with NBT on real samples/parts in combination with the finite element method; such models can be designed and developed with respect to dynamic recrystallization and grain growth phenomena.

5. Conclusions

HT parameters have an influence on specimen microstructure and final ADI properties. Besides HT temperatures and times, DCI chemical composition is also very important.

In industry, tempering HT is used to decrease the brittleness of the material and eliminate RS. Tensile strength and elongation are increased. The final mechanical properties of the material rely on tempering temperature and time, as well as the weight percentages of the alloying elements.

Phases of ausferrite and graphite spheres are visible under all magnifications. Looking at the microstructure of the specimens with subsequent tempering, they appear more needle-like, while the specimens without subsequent tempering have a more plate-like character. In addition, ferrite phases are also visible in the material at $500\times$ magnification for the specimens without subsequent tempering, while ferrite phases are minimal in the specimens with subsequent tempering. The subsequent tempering resulted in a more uniform microstructure between the different specimens, which is confirmed by the results: better mechanical properties were obtained. It is believed that during subsequent tempering, the ausferrite began to disintegrate due to C diffusion and partially transformed into pearlite and carbides, which is why there was an improvement in hardness and elongation

and a slight decrease in tensile strength for specimen sets 719, 720 and 721, while tensile strength increased for specimen sets 722 and 724.

After subsequent tempering, the tensile strength decreased at tempering temperatures of 250 and 331 °C and increased at 420 °C compared to the tensile strength of the specimens without subsequent tempering. Elongation also significantly increased. The reason for the better mechanical properties are changes in the microstructure of the specimens during subsequent tempering. It is believed that the obtained microstructure is more homogeneous with uniform ausferrite and contains fewer ferritic phases, therefore resulting in more even properties.

Maximum tensile strength of 1023 MPa and the lowest elongation was measured on specimen set 719, obtained at 250 °C and 30 min. Lowest tensile strength of 814 MPa had specimen set 721, austempered at 331 °C for 68 min. Specimen set 722 had the highest elongation of 30.2%, which was annealed at 420 °C for 30 min.

Hardness increased for all specimens with subsequent annealing. The greatest change in hardness was observed in specimen set 721 compared to specimen set 706: 86 HV. Specimen set 719 had the highest hardness and specimen set 722 had the lowest hardness. The reason for the increase in hardness is the formation of secondary carbides in the microstructure due to C diffusion from decomposed ausferrite during the subsequent tempering process. These carbides are relatively small and uniformly distributed in the microstructure, as can be seen from the micrographs, which increase the hardness.

Since this is a novel double annealing HT of ADI and there is no research on this topic to date. It would be useful to further apply NBT to obtain complementary information on the nano-(micro-)structure related to the phases formed after subsequent annealing.

Author Contributions: Conceptualization, N.Č. and H.A.; methodology, N.Č.; software, N.Č. and K.G.; validation, N.Č., M.R. and H.A.; formal analysis, K.G.; investigation, N.Č. and K.G.; resources, N.Č. and K.G.; data curation, N.Č. and H.A.; writing—original draft preparation, N.Č. and M.R.; writing—review and editing, N.Č. and M.R.; visualization, N.Č. and K.G.; supervision, M.R. and H.A. All authors have read and agreed to the published version of the manuscript.

Funding: This research received no external funding.

Data Availability Statement: The data presented in this study are available on request from the corresponding author.

Conflicts of Interest: The authors declare no conflict of interest.

References

1. Labercque, C.; Gagne, M. *Ductile Iron—Fifty Years of Continued Development*; Rio Tinto Iron & Titanium: Sorel-Tracy, QC, Canada, 1998.
2. Žmak, I. Modeling the Structure and Properties of Ductile Cast Iron by Neural Networks. Ph.D. Thesis, Faculty of Mechanical Engineering and Naval Architecture, Zagreb, Croatia, 2008.
3. Global Casting Production Trend and Conclusion in 2014. Available online: https://www.pinepacific.com/news_detail.php?idnews=93 (accessed on 2 August 2023).
4. Bendikiene, R.; Ciuplys, A.; Cesnavicius, R.; Jutas, A.; Bahdanovich, A.; Marmysh, D.; Nasan, A.; Shemet, L.; Sherbakov, S. Influence of Austempering Temperatures on the Microstructure and Mechanical Properties of Austempered Ductile Cast Iron. *Metals* **2021**, *11*, 967. [[CrossRef](#)]
5. Akinribide, O.J.; Ogundare, O.D.; Oluwafemi, O.M.; Ebisike, K.; Nageri, A.K.; Akinwamide, S.O.; Gamaoun, F.; Olubambi, P.A. A Review on Heat Treatment of Cast Iron: Phase Evolution and Mechanical Characterization. *Materials* **2022**, *15*, 7109. [[CrossRef](#)] [[PubMed](#)]
6. Landesberger, M.; Koos, R.; Hofmann, M.; Li, X.; Boll, T.; Petry, W.; Volk, W. Phase Transition Kinetics in Austempered Ductile Iron (ADI) with Regard to Mo Content. *Materials* **2020**, *13*, 5266. [[CrossRef](#)] [[PubMed](#)]
7. Tyrała, E.; Górný, M.; Kawalec, M.; Muszyńska, A.; Lopez, H.F. Evaluation of Volume Fraction of Austenite in Austempering Process of Austempered Ductile Iron. *Metals* **2019**, *9*, 893. [[CrossRef](#)]
8. Bai, J.; Xu, H.; Wang, Y.; Chen, X.; Zhang, X.; Cao, W.; Xu, Y. Microstructures and Mechanical Properties of Ductile Cast Iron with Different Crystallizer Inner Diameters. *Crystals* **2022**, *12*, 413. [[CrossRef](#)]

9. Hsu, C.-H.; Lin, C.-Y.; You, W.-S. Microstructure and Dry/Wet Tribological Behaviors of 1% Cu-Alloyed Austempered Ductile Iron. *Materials* **2023**, *16*, 2284. [[CrossRef](#)]
10. *ASM Metals Handbook Volume 04—Heat Treatment*; Heat Treating of Ductile Irons. ASM International: Almere, The Netherlands, 1991; p. 1498.
11. Elliot, R. The role of research in promoting austempered ductile iron. *Heat Treat. Met.* **1997**, *24*, 55–59.
12. Chandler, H. *Heat Treating Guide: Practices and Procedures for Irons and Steels*, 2nd ed.; ASM International: Almere, The Netherlands, 1994.
13. Čatipović, N. Influence of Copper and Heat Treatment on the Properties of Austempered Ductile Iron. Ph.D. Thesis, Faculty of Electrical Engineering, Mechanical Engineering and Naval Architecture, Split, Croatia, 2018.
14. Foundry Industry 2020: Trends and Challenges. Available online: https://www.heat-processing.com/fileadmin/HPO/Dateien_Redaktion/Selected_Reports/150616_GIFA_Presentation_EN.pdf (accessed on 4 August 2023).
15. Sponseller, D.L.; Scholz, W.G.; Rundle, D.F. Development of Low-Alloy Ductile Irons for Service at 1200–1500 F. *AFS Trans.* **1968**, *76*, 353–368.
16. Sahoo, S.K. *A Study on the Effect of Austempering Temperature, Time and Copper Addition on the Mechanical Properties of Austempered Ductile Iron*; NIT: Rourkela, India, 2012.
17. Cast Metals Development Ltd, Austempered ductile-iron castings—Advantages, production, properties and specifications. *Mater. Des.* **1992**, *13*, 285–297. [[CrossRef](#)]
18. Keough, J.R.; Hayrynen, K.L.; Pioszak, G.L. *Designing with Austempered Ductile Iron (ADI)*; Applied Process Inc., Technologies Division: Livonia, MI, USA; University of Michigan: Ann Arbor, MI, USA, 2010.
19. Nofal, A. *Austempered Ductile Iron (ADI) Production, Properties and Applications*; CMRDI: Kairo, Egypt, 2014.
20. Stupnišek, M.; Cajner, F. *Basics of Metal Heat Treatment*; University of Zagreb: Zagreb, Croatia, 2001.
21. Engels, G. Half a century of foundry technical progress in the mirror of GIFA. In Proceedings of the 43rd Foundry Conference, Portorož, Slovenija, 18–19 September 2003.
22. Druschitz, A.P.; Aristizabal, R.E.; Druschitz, E.; Hubbard, C.R.; Watkins, T.R.; Walker, L.; Ostrander, M. In-Situ Studies of Intercritically Austempered Ductile Iron (IADI) Using Neutron Diffraction. *Metall. Mater. Trans. A* **2012**, *43*, 1468–1476. [[CrossRef](#)]
23. Druschitz, A.; Aristizabal, R.; Druschitz, E.; Hubbard, C.; Watkins, T. Neutron Diffraction Studies of Intercritically Austempered Ductile Irons. *SAE Int. J. Mater. Manuf.* **2011**, *4*, 111–118. [[CrossRef](#)]
24. Li, X.; Soria, S.; Gan, W.; Hofmann, M.; Schulz, M.; Hoelzel, M.; Brokmeier, H.-G.; Petry, W. Multi-scale phase analyses of strain-induced martensite in austempered ductile iron (ADI) using neutron diffraction and transmission techniques. *J. Mater. Sci.* **2012**, *56*, 5296–5306. [[CrossRef](#)]
25. Čatipović, N.; Živković, D.; Rogante, M. *Influenza della Temperatura sulla Microstruttura della Ghisa Duttile Austemperata*; Tecniche Nuove, Ed.; Fonderia Pressofusione: Milano, Italy, 2018; Volume 2, pp. 30–33.
26. Dubal, G.P. The Basics of Molten Salt Quenchant. *Mater. Proc. Forum* **2003**, *3*, 23–27.
27. Yescas, M.A.; Bhadeshia, H.K.D.H.; MacKay, D.J. Estimation of the amount of retained austenite in austempered ductile irons using neural networks. *Mater. Sci. Eng. A* **2001**, *311*, 162–173. [[CrossRef](#)]
28. Li, X.H.; Saal, P.; Gan, W.M.; Landesberger, M.; Hoelzel, M.; Hofmann, M. Strain Induced Martensitic Transformation in Austempered Ductile Iron (ADI). *J. Phys. Conf. Ser.* **2016**, *746*, 012055. [[CrossRef](#)]
29. Sellamuthu, P.; Samuel, D.G.H.; Dinakaran, D.; Premkumar, V.P.; Li, Z.; Seetharaman, S. Austempered Ductile Iron (ADI): Influence of Austempering Temperature on Microstructure, Mechanical and Wear Properties and Energy Consumption. *Metals* **2018**, *8*, 53. [[CrossRef](#)]
30. Meier, L.; Hofmann, M.; Saal, P.; Volk, W.; Hoffmann, H. In-situ measurement of phase transformation kinetics in austempered ductile iron. *Mater. Charact.* **2013**, *85*, 124–133. [[CrossRef](#)]
31. Čatipović, N.; Živković, D.; Dadić, Z.; Krolo, J. Influence of austempering temperature and salt bath agitation on microstructure and mechanical properties of austempered ductile iron. *Kov. Mater.* **2018**, *56*, 137–144.
32. Behera, G.; Sohala, S.R. Effect of Copper on the Properties of Austempered Ductile Iron Castings. Bachelor's Thesis, Department of Metallurgical and Materials Engineering, National Institute of Technology, Rourkela, India, 2012.
33. Sharma, A.; Singh, K.K.; Gupta, G.K. Study on the Effects of Austempering Variables and Copper Addition on Mechanical Properties of Austempered Ductile Iron. In Proceedings of the 6th International & 27th All India Manufacturing Technology, Design and Research Conference (AIMTDR-2016), Pune, India, 16–18 December 2016.
34. Sidjanin, L.; Smallman, R.E. Metallography of bainitic transformation in austempered ductile iron. *Mater. Sci. Technol.* **1992**, *8*, 1095–1103. [[CrossRef](#)]
35. Rogante, M. Caratterizzazione, mediante scattering neutronico, di materiali e componenti per l'impiantistica nucleare ed industrial. Ph.D. Thesis, Nuclear Engineering, University of Bologna, Bologna, Italy, 1999; p. 223.
36. Rogante, M. *Industrial Applications of Neutron Techniques, Proc. 1^o National Workshop for Industry*; Rogante Engineering, Ed.; Applicazioni Industriale delle Tecniche Neutroniche®: Civitanova Marche, Italy, 2008; pp. 40–120.
37. Caratterizzazione di materiali e Componenti a Livello di Micro- e Nano-Scala Mediante Diffusione Neutronica a Piccoli Angoli; Studio d'Ingegneria ROGANTE: Civitanova Marche, Italy, 2008. Available online: http://www.roganteengineering.it/pagine_servizi/servizi2.pdf (accessed on 8 August 2023).

38. Dojcinovic, M.; Eric, O.; Rajnovic, D.; Sidjanin, L.; Balos, S. Effect of austempering temperature on cavitation behaviour of unalloyed ADI material. *Mater. Charact.* **2013**, *82*, 66–72. [[CrossRef](#)]
39. Determinazione delle Tensioni Residue Mediante Diffrazione Neutronica; Studio d'Ingegneria Rogante: Civitanova Marche, Italy. 2008. Available online: http://www.roganteengineering.it/pagine_servizi/servizi1.pdf (accessed on 8 August 2023).

Disclaimer/Publisher's Note: The statements, opinions and data contained in all publications are solely those of the individual author(s) and contributor(s) and not of MDPI and/or the editor(s). MDPI and/or the editor(s) disclaim responsibility for any injury to people or property resulting from any ideas, methods, instructions or products referred to in the content.